

Strain energy enhanced room-temperature magnetocaloric effect in Mn_5Ge_3

Xiaohe Liu(刘潇贺), Ping Song(宋平), Sen Yao(姚森), Yuhao Lei(雷雨豪), Ling Yang(杨玲), Shenxiang Du(杜深祥), Yiran Deng(邓贻然), and Defeng Guo(郭得峰)

Citation: Chin. Phys. B, 2026, 35 (**2**): 027505. DOI: 10.1088/1674-1056/adf6a6
http://cpb.iphy.ac.cn; http://iopscience.iop.org/cpb

What follows is a list of articles you may be interested in

Tuning the magnetocaloric and structural properties of $La_{0.67}Sr_{0.28}Pr_{0.05}Mn_{1-x}Co_xO_3$ refrigeration materials

Changji Xu(徐长吉), Xinyu Jiang(姜心雨), Zhengguang Zou(邹正光), Zhuojia Xie(谢卓家), Weijian Zhang(张伟建), and Min Feng(冯敏)

Chin. Phys. B, 2024, 33 (**12**): 127501. DOI: 10.1088/1674-1056/ad8550

Magnetic and magnetocaloric effect of $Er_{20}Ho_{20}Dy_{20}Cu_{20}Ni_{20}$ high-entropy metallic glass

Shi-Lin Yu(于世霖), Lu Tian(田路), Jun-Feng Wang(王俊峰), Xin-Guo Zhao(赵新国), Da Li(李达), Zhao-Jun Mo(莫兆军), and Bing Li(李昺)

Chin. Phys. B, 2024, 33 (**5**): 057502. DOI: 10.1088/1674-1056/ad1a94

Mechanical and magnetocaloric adjustable properties of Fe_3O_4/PET deformed nanoparticle film

Fengguo Fan(范凤国) and Lintong Duan(段林彤)

Chin. Phys. B, 2024, 33 (**3**): 037502. DOI: 10.1088/1674-1056/acf280

Giant low-field cryogenic magnetocaloric effect in polycrystalline $LiErF_4$ compound

Zhaojun Mo(莫兆军), Jianjian Gong(巩建建), Huicai Xie(谢慧财), Lei Zhang(张磊), Qi Fu(付琪), Xinqiang Gao(高新强), Zhenxing Li(李振兴), and Jun Shen(沈俊)

Chin. Phys. B, 2023, 32 (**2**): 027503. DOI: 10.1088/1674-1056/ac65ef

Magnetocaloric properties of phenolic resin bonded $La(Fe,Si)_{13}$-based plates and its use in a hybrid magnetic refrigerator

Shao-Shan Xu(徐少山), Qi Fu(付琪), Yi-Fan Zhou(周益帆), Ling Peng(彭铃), Xin-Qiang Gao(高新强), Zhen-Xing Li(李振兴), Mao-Qiong Gong(公茂琼), Xue-Qiang Dong(董学强), and Jun Shen(沈俊)

Chin. Phys. B, 2023, 32 (**2**): 027502. DOI: 10.1088/1674-1056/ac9fbf

---

Strain energy enhanced room-temperature magnetocaloric effect in Mn_5Ge_3

Xiaohe Liu(刘潇贺)[1,2], Ping Song(宋平)[1,2,†], Sen Yao(姚森)[1,2], Yuhao Lei(雷雨豪)[1,2], Ling Yang(杨玲)[1,2], Shenxiang Du(杜深祥)[1,2], Yiran Deng(邓贻然)[1,2], and Defeng Guo(郭得峰)[1,2]

[1] *Center for Extreme Deformation Research, State Key Laboratory of Metastable Materials Science and Technology, Yanshan University, Qinhuangdao* 066004, *China*

[2] *Key Laboratory for Microstructural Material Physics of Hebei Province, School of Science, Yanshan University, Qinhuangdao* 066004, *China*

(Received 19 May 2025; revised manuscript received 14 July 2025; accepted manuscript online 1 August 2025)

Large magnetic entropy change (ΔS_M) can realize a prominent heat transformation under the magnetic field and directly strengthen the efficacy of the magnetocaloric effect, which provides a pioneering environmentally friendly solid-state strategy to improve refrigeration capacities and efficiencies. The second-order magnetic transition (SOMT) materials have broader ΔS_M peaks without thermal hysteresis, making them highly attractive in magnetic refrigeration, especially in the room temperature range. Here, we report a significant enhancement of ΔS_M at room temperature in single-crystal Mn_5Ge_3. In this SOMT system, we realize a 60% improvement of $-\Delta S_M^{max}$ from 3.5 J/kg·K to 5.6 J/kg·K at $T = 300$ K. This considerable enhancement of ΔS_M is achieved by intentionally introducing strain energy through high-pressure constrained deformation. Both experimental results and Monte Carlo simulations demonstrate that the enhancement of ΔS_M originates from the microscopic strain and lattice deformation induced by strain energy after deformation. This strain energy will reconstruct the energy landscape of this ferromagnetic system and enhance magnetization, resulting in a giant intensity of magnetocaloric responses. Our findings provide an approach to increase magnetic entropy change and may give fresh ideas for exploring advanced magnetocaloric materials.

Keywords: magnetocaloric effect, magnetic entropy change, second-order magnetic transition, strain energy, deformation

PACS: 75.30.Sg, 62.20.F–, 75.47.Np

DOI: 10.1088/1674-1056/adf6a6 **CSTR:** 32038.14.CPB.adf6a6

1. Introduction

The magnetocaloric effect (MCE), characterized by isothermal magnetic entropy change or adiabatic temperature change of magnetic materials under the application of an external magnetic field, provides a pioneering environmentally friendly solid-state strategy to improve refrigeration capacities and efficiencies.[1–4] The room-temperature magnetic refrigeration based on MCE is of special interest because of its great social and economic benefits.[1] Therefore, since Brown observed the large MCE near room temperature ($T_C = 293$ K) for Gd,[5] magnetic materials exhibiting a large MCE have been widely explored in the vast family of pure elements and compounds, ranging from rare earth materials to transition metal alloys, from bulk samples to nanoparticles, from single-phase materials to multiphase compounds,[6–8] which can be classified into first-order magnetic transition (FOMT) materials and second-order magnetic transition (SOMT) materials according to their phase transition order.[9,10]

The SOMT materials have broader magnetic entropy change (ΔS_M) peaks without thermal hysteresis, making them highly attractive in magnetic refrigeration, especially in the room temperature range.[11,12] The fly in the ointment is that the SOMT materials usually possess low values of ΔS_M at operating temperatures. To date, researchers are still making efforts to explore the new SOMT materials with large ΔS_M mainly by component optimization and microstructure modification.[11,13–18] However, improving the inherent shortage of magnetocaloric responses at room temperature is still one of the enormous challenges for SOMT materials.

In this paper, we report a strategy to increase the magnetic entropy change of SOMT materials by intentionally enhancing the intensity of magnetization with high-pressure constrained deformation. The power of this anisotropic severe plastic deformation technique has also been verified in constructing high-performance permanent magnetic materials and antiferromagnetic materials.[19–29] Recently, this technique has achieved a breakthrough in the fast fabrication of multifunctional ferromagnets and led to the discovery of a class of multifunctional high-temperature ferromagnetic materials with an exceptional combination of high energy product, large electrical resistivity, and superior thermal stability of coercivity.[20]

To demonstrate the efficacy of this strategy in the field of magnetocaloric materials, we select single crystal Mn_5Ge_3 as the model material. In this SOMT system, Mn and Ge atoms crystallize in the hexagonal space group $P6_3/mcm$ with Mn occupying two different Wyckoff positions of 4*d* and 6*g*

†Corresponding author. E-mail: psong@ysu.edu.cn

© 2026 Chinese Physical Society and IOP Publishing Ltd. All rights, including for text and data mining, AI training, and similar technologies, are reserved.

sites and Ge occupying 6*g* sites,[30] as shown in Fig. S1 (in the supporting information). In this configuration, two different magnetic moments of Mn atoms align parallel to the hexagonal *c*-axis, forming a collinear ferromagnetic structure with a Curie temperature near 296 K.[12] These characteristics make Mn_5Ge_3 a model material for studying the MCE at room temperature.[31–33] The applied high-pressure constrained deformation will reconstruct the energy landscape of this ferromagnetic system by introducing strain energy. The additional strain energy will generate an enhancement in magnetization. As a result, we realize a 60% improvement of $-\Delta S_{\rm M}^{\rm max}$ from 3.5 J/kg·K to 5.6 J/kg·K at $T = 300$ K. Our findings provide an approach to increase magnetic entropy change and may give fresh ideas for exploring advanced magnetocaloric materials.

2. Experimental section

2.1. Materials synthesis

Mn_5Ge_3 single crystals were synthesized using the bismuth-flux growth method. Mn (99.98%), Ge (99.999%), and Bi (99.99%) were mixed in a stoichiometric ratio of 5:3:55 and placed in an alumina crucible sealed into a quartz tube under vacuum. The quartz tube was heated to 1323 K in 10 hours and held for 72 hours. The temperature was slowly cooled to 923 K at a rate of 2 K/h. The Mn_5Ge_3 single crystals were then centrifugally separated from the bismuth flux using an embedded corundum filter. The composition stoichiometry was checked by energy-dispersive x-ray (EDX) spectroscopy combined with scanning electron microscopy (SEM) (S-4800, HITACHI).

2.2. High-pressure constrained deformation

The deformations were carried out using a commercial 600-kN machine. The power of this anisotropic severe plastic deformation technique has also been verified in constructing high-performance magnetic materials.[20,21] The process of high-pressure constrained deformation for the Mn_5Ge_3 single crystals is sketched in Fig. S2. The hexagonal Mn_5Ge_3 single crystals were placed into the stacked steel wafers. Then, the steel wafers were sealed in a steel capsule. A press was applied to the assembled sample to realize the high-pressure constrained deformation. The press direction parallels the $[10\bar{1}0]$ crystal orientation. The strength of deformation was expressed in terms of stress (σ) and the corresponding macro-strain (ε) along the direction of stress. Finally, the deformed sample was separated from the steel capsule and polished.

2.3. Structural characterization

The crystal structure of the single-crystal Mn_5Ge_3 was characterized by x-ray diffraction (XRD) with Co $K\alpha$ radiation ($\lambda = 1.789$ Å) in a step-scanning mode (PIXcel-3D, PANalytical B.V., Inc.). The microstructure of samples was characterized by transmission electron microscopy (TEM) (JEM-2100 Plus, JEOL).

2.4. Magnetization measurement

Isothermal initial magnetization curves of samples were measured along the stress direction using a vibrating sample magnetometer (VSM) (Model-7404, 1.6 T, 263 K–773 K, Lakeshore). The magnetic entropy change ($\Delta S_{\rm M}$) was calculated by $\Delta S_{\rm M} = \int_0^H (\partial M/\partial T)\,{\rm d}H$.

2.5. Monte Carlo simulation

Monte Carlo simulations were performed using the Ising-like Hamiltonian $\mathcal{H} = -\sum_{i\neq j} J_{ij}\boldsymbol{S}_i\cdot\boldsymbol{S}_j - \boldsymbol{h}\cdot\sum_i g_i\boldsymbol{S}_i - E_u$, where J_{ij} is the exchange constant between the spins $\boldsymbol{S}_i$ and $\boldsymbol{S}_j$, $\boldsymbol{h}$ is the external magnetic field, g_i is the Lande factor, and E_u is the strain energy. For Mn1 (4*d* sites), $S = \pm 1.5$, while for Mn2 (6*g* sites), $S = \pm 1.0$, and $g = 2.06$ for both the Mn1 and Mn2. For the exchange constant, we assign $J_{\rm dd}$ for Mn1–Mn1, $J_{\rm gg}$ for Mn2–Mn2, and $J_{\rm dg}$ for Mn1–Mn2, respectively. The software package used for the theoretical calculations here is Matlab R2020a. During the simulation, we scale the exchange constants $J_{\rm gg}$ and $J_{\rm dg}$, the temperature (T), the external magnetic field (h), and the strain energy (E_u) to $J_{\rm dd}$. We construct a 1000-cell superlattice with periodic boundary conditions and select $J_{\rm dd} = 2.44$ meV, $J_{\rm gg} = 1.875J_{\rm dd}$, and $J_{\rm dg} = 1.221J_{\rm dd}$. The value of E_u is chosen based on empiricism. The number of iterations is 50000 times.

3. Results and discussion

According to the Maxwell's relation, $(\partial S/\partial H)_T = (\partial M/\partial T)_H$, the magnetic entropy change ($\Delta S_{\rm M}$) can be obtained as[1]

$$\Delta S_{\rm M} = \int_0^H \frac{\partial M}{\partial T}\,{\rm d}H, \tag{1}$$

where M is the magnetization, T is the temperature, and H is the external magnetic field. Equation (1) indicates that the increase in the magnitude of M will result in a corresponding enlargement of $\Delta S_{\rm M}$. Therefore, to achieve a significant $\Delta S_{\rm M}$, we can design experimental strategies to increase the value of M. Our previous work demonstrates a feasible way to increase magnetization by introducing strain energy.[28,34] In this way, we may also achieve a large $\Delta S_{\rm M}$ by realizing the increase of M via the introduction of strain energy in the SOMT materials.

Figure 1 shows the concept of strain energy to enhance the magnetic entropy change in Mn_5Ge_3. According to the ferromagnetic thermodynamics of the Ising model, the magnetization (M) is a derivative of the total energy (E) of the external magnetic field (H).[35] For the regular Mn_5Ge_3 crystal, the total energy E includes exchange energy E_1 and Zeeman energy E_2 [Fig. 1(a)]. When we introduce a lattice deformation, as shown in Fig. 1(b), an additional strain energy (E_u) will arise

from the lattice deformation. This appropriate E_u may lead to an increase in magnetization [Fig. 1(c)]. As a result, we can realize a rise in ΔS_M [Fig. 1(d)]. It is worth noting that the strain may increase or decrease magnetization or even destroy the magnetic ordering. The excessive strain can also lead to a decrease in ΔS_M. In this paper, we introduce the appropriate strain energy without damaging the integrity and crystal structure of the samples.

Based on this idea, we design and experimentally introduce the strain energy in Mn_5Ge_3 by high-pressure constrained deformation. We first synthesize the Mn_5Ge_3 single crystals using the bismuth-flux method. The obtained Mn_5Ge_3 single crystals are in the form of a hexagonal prism, as shown in Fig. S1. Figure S2 sketches the process of high-pressure constrained deformation for the Mn_5Ge_3 single crystals. The stress of deformation (σ) varies from 0 to 1.24 GPa, and the corresponding macro-strain (ε) ranges from 0 to 28%. The morphology of the deformed Mn_5Ge_3 single crystals is shown in Fig. S3. The energy-dispersive x-ray (EDX) measurement reveals a chemical composition of $Mn_{5.35}Ge_{2.84}$ for the as-prepared sample and $Mn_{5.35}Ge_{2.75}$ for the deformed sample (Fig. S4). We refer to our samples as Mn_5Ge_3 in the following.

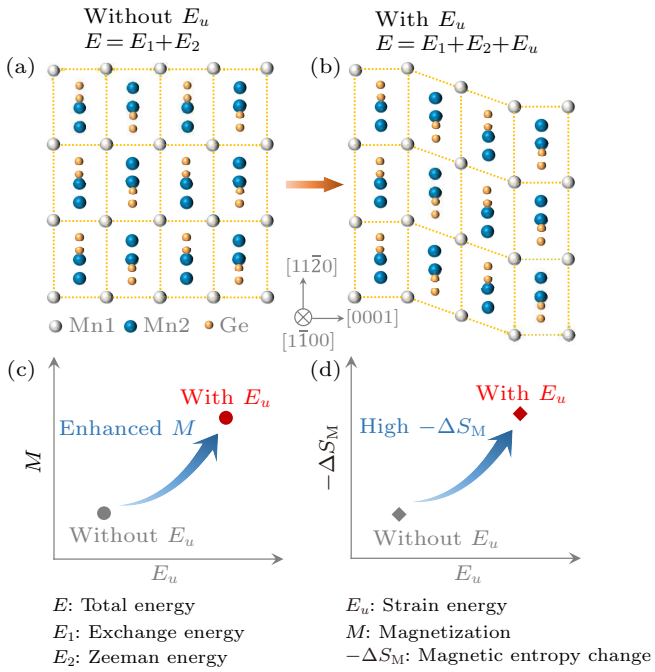


Fig. 1. Concept of strain energy to enhance the magnetic entropy change in Mn_5Ge_3. Schematic diagram of the atomic configuration (a) without strain energy and (b) with strain energy on the $(1\bar{1}00)$ plane. Schematic representation of the impact of strain energy on (c) magnetization and (d) magnetic entropy change.

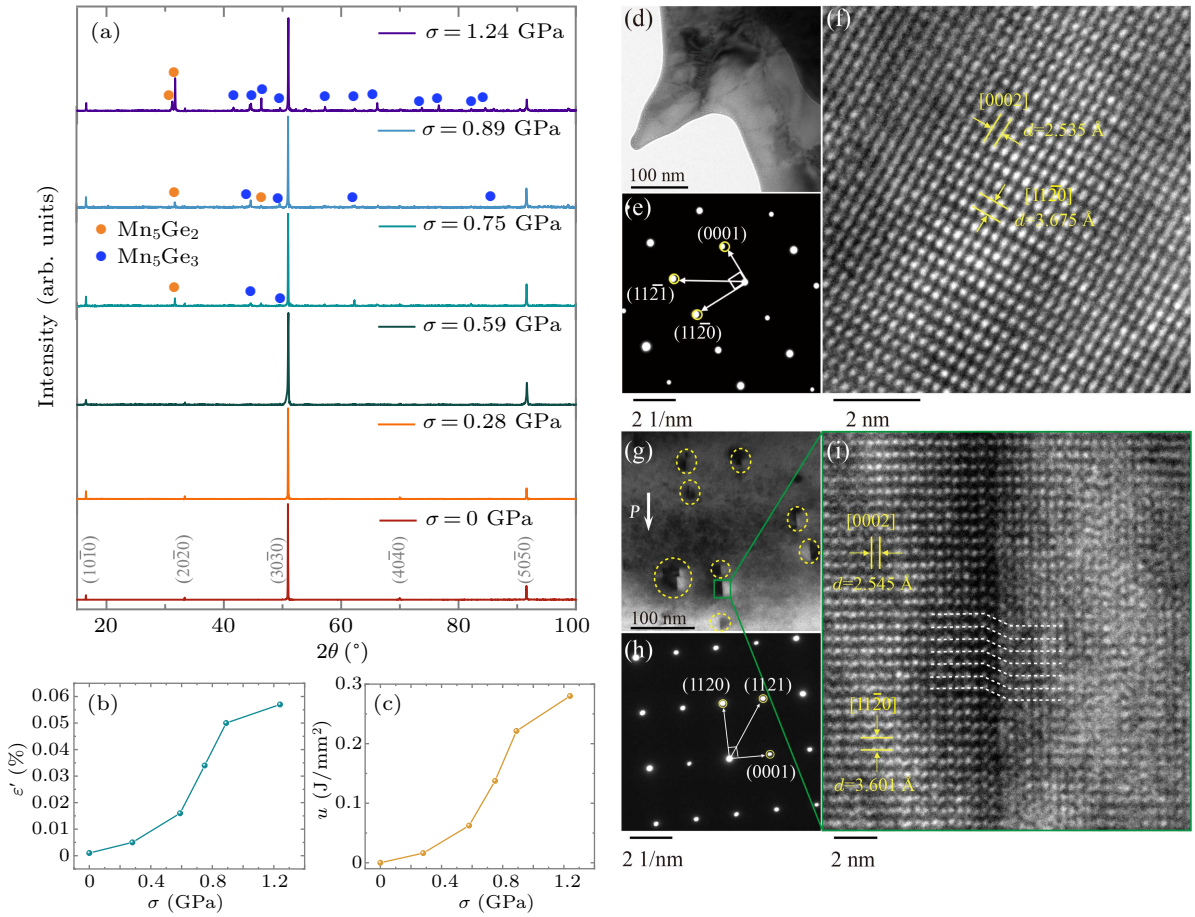


Fig. 2. Crystal structure and microstructure of Mn_5Ge_3 single crystals before and after deformation. (a) XRD patterns with different stress (σ) measured parallel to $[10\bar{1}0]$ direction. (b) The microscopic strain (ε') fitted by XRD patterns and (c) the corresponding strain energy density (u) after the deformation at different σ. (d)–(e) TEM image and SAED pattern of the as-prepared Mn_5Ge_3. (f) High-resolution TEM (HRTEM) image of the as-prepared Mn_5Ge_3. (g)–(h) TEM image and SAED pattern of the cross-section along the stress direction at $\sigma = 0.75$ GPa. (i) HRTEM image of the marked area in panel (g). White dash lines are to guide the eye to the lattice planes.

Figure 2(a) shows the XRD patterns of Mn_5Ge_3 at various values of σ. There are no extra diffraction peaks except $\{10\bar{1}0\}$ lattice planes that appear in the XRD patterns when $\sigma \leq 0.59$ GPa, indicating the single-crystal stability of Mn_5Ge_3 during the deformation process. With the increase in σ, the diffraction peaks of some other lattice planes and a new phase of Mn_5Ge_2 begin to appear at $\sigma = 0.75$ GPa. When $\sigma = 1.24$ GPa, the single-crystal sample shows an obvious poly-crystallization. By fitting the XRD patterns, we achieve the microscopic strain (ε') of the deformed samples at different σ. As shown in Fig. 2(b), the value of ε' has a monotonic increase with the increase of σ. The strain energy density (u), ε', and σ are related as $u = \varepsilon'\sigma$.[36] The calculated value of u has the same monotonically increasing trend as the increase in σ [Fig. 2(c)]. The result of σ dependence of ε' and u indicates that strain energy is introduced into the sample by deformation.

To investigate the effect of the deformation process on the essence of the samples, we characterize the microstructure of Mn_5Ge_3 before and after deformation. Figures 2(d)–2(f) show the transmission electron microscopy (TEM) image and selected area electron diffraction (SAED) pattern of the as-prepared Mn_5Ge_3 single crystals. The as-prepared single-crystal samples have a regular lattice arrangement without defects. In contrast, the deformed sample at $\sigma = 0.75$ GPa shows a prominent lattice deformation as marked by dash lines in Fig. 2(g), although the SAED pattern shows a single-crystal characteristic [Fig. 2(h)]. The high-resolution TEM (HRTEM) image of the deformed sample shows that the lattice planes of $(11\bar{2}0)$ have apparent slip along the direction parallel to the stress [Fig. 2(i)]. The prominent lattice deformation of the deformed samples may be facilitated by the enhanced strain energy under high stress and strain.[21] It should be noted that the HRTEM cross-section image of the deformed sample is not entirely along the pressure direction ($[10\bar{1}0]$ crystal direction). This is due to the deviation caused by the limitation of experimental conditions in sample preparation.

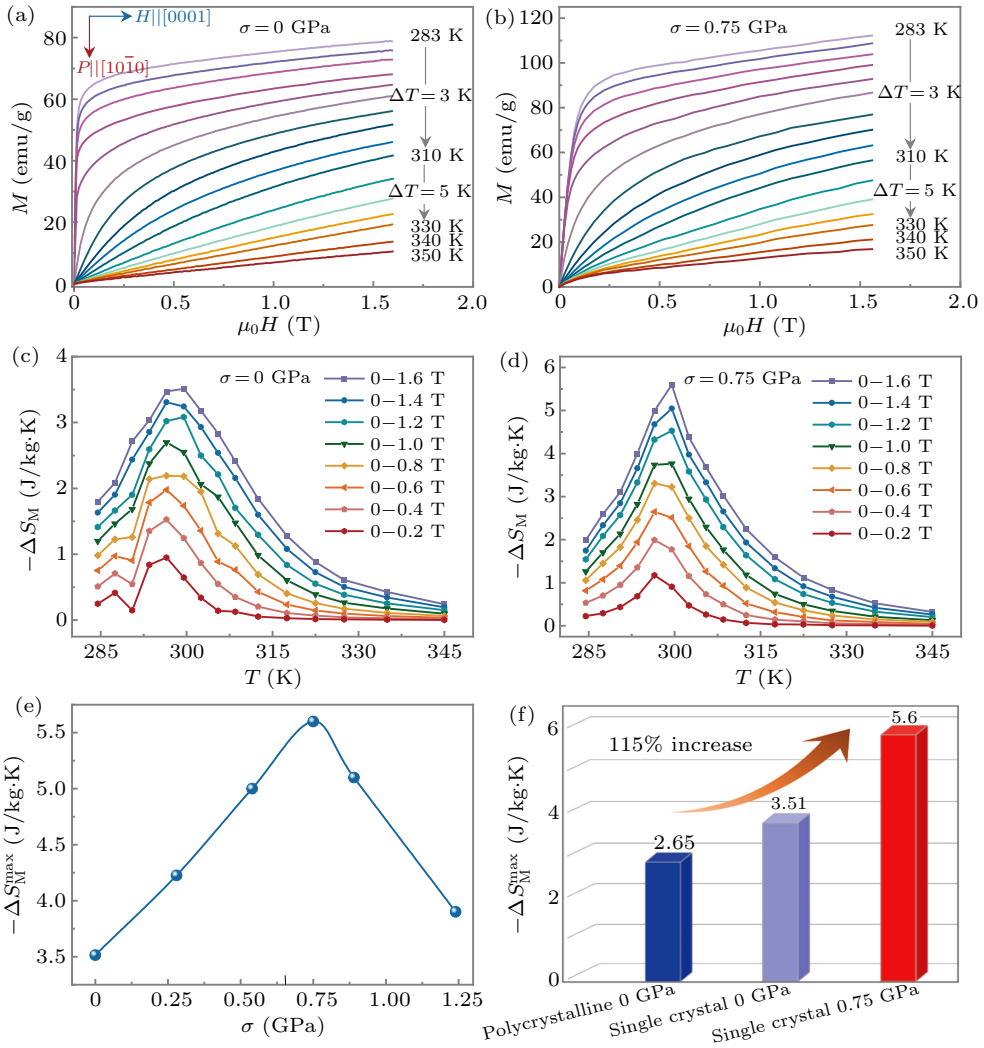


Fig. 3. Enhanced magnetocaloric effect of Mn_5Ge_3 single crystals. (a)–(b) External magnetic field dependence of magnetization for the as-prepared sample ($\sigma = 0$ GPa) and deformed sample ($\sigma = 0.75$ GPa) at different temperatures. For all the measurements, H parallels [0001] direction. (c)–(d) Temperature dependence of magnetic entropy change $-\Delta S_M$ for the as-prepared sample ($\sigma = 0$ GPa) and deformed sample ($\sigma = 0.75$ GPa) under different external magnetic fields. (e) Stress dependence of maximum magnetic entropy change $-\Delta S_M^{max}$ for Mn_5Ge_3. (f) Comparison of $-\Delta S_M^{max}$ of polycrystalline (PC) Mn_5Ge_3, single-crystal (SC) Mn_5Ge_3, and deformed SC Mn_5Ge_3.

Table 1. T_C and $|-\Delta S_M^{max}|$ of Gd and Mn_5Ge_3-based compounds.

Material	σ (GPa)	T_C (K)	ΔH (T)	$\lvert-\Delta S_M^{max}\rvert$ (J·kg^{-1}·K^{-1})	Ref.
Mn_5Ge_3	0	298	1.6	3.5	this work
Mn_5Ge_3	0.28	298	1.6	4.2	this work
Mn_5Ge_3	0.54	298	1.6	5	this work
Mn_5Ge_3	0.75	299	1.6	5.6	this work
Mn_5Ge_3	0.89	299	1.6	5.1	this work
Mn_5Ge_3	1.24	299	1.6	3.9	this work
Mn_5Ge_3	–	296	1	2.7	[37]
Gd	–	295	2	6.1	[38]
$Mn_5Ge_{2.5}Si_{0.5}$	–	299	1	2.1	[39]
$Mn_5Ge_{2.7}Sb_{0.3}$	–	312	2	2.9	[31]
$Mn_{4.75}Fe_{0.25}Ge_3$	–	311	1	1.6	[40]

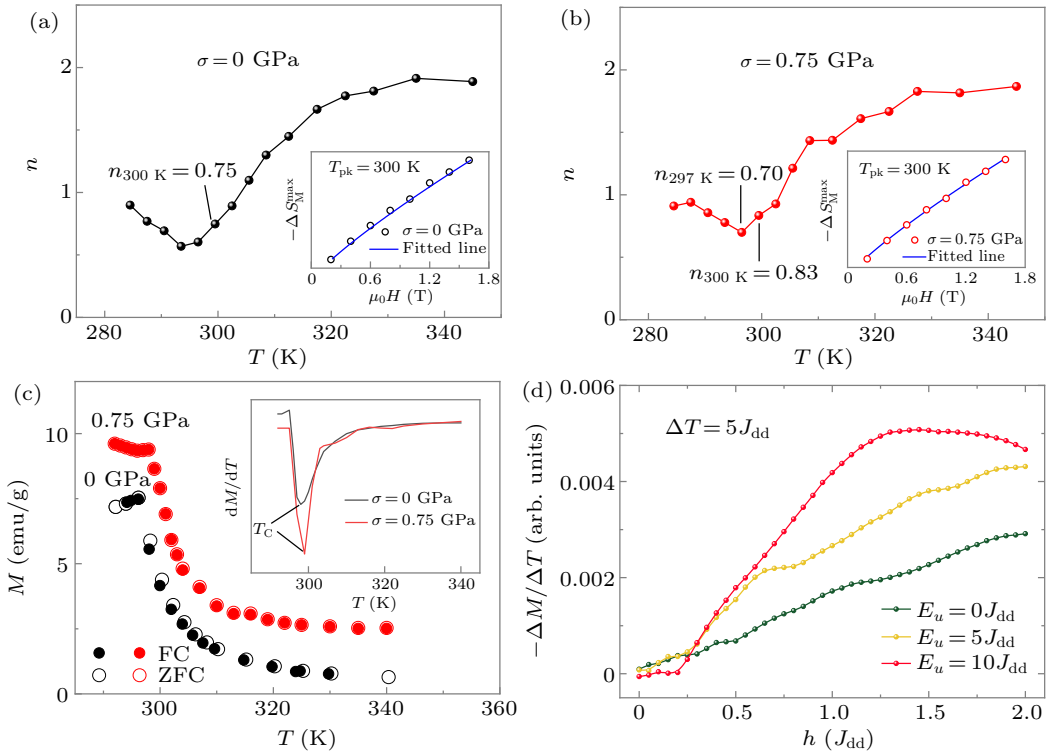


Fig. 4. Temperature dependence of the power exponent characterizing the field dependence of $-\Delta S_M$ for (a) the as-prepared sample ($\sigma = 0$ GPa) and (b) deformed sample ($\sigma = 0.75$ GPa). Insets show the power law behavior of maximum entropy change at $T_{pk} = 300$ K for as-prepared and deformed samples. (b) Temperature dependence of magnetization with different stresses ($\sigma = 0$ GPa and 0.75 GPa) of the Mn_5Ge_3 single crystals at $H = 500$ Oe (1 Oe = 79.5775 A·m^{-1}). Solid dots and open circles represent the field cooling (FC) and zero-field cooling (ZFC) processes. For all the measurements, H parallels the [0001] direction. The inset shows the corresponding derivatives of the FC M–T curves. (c) Simulated $-\Delta M/\Delta T$ of Mn_5Ge_3 with different $E_u = 0\ J_{dd}$, 5 J_{dd}, and 10 J_{dd}. h is the external magnetic field reduced by J_{dd}.

Figure 3 shows the results of ΔS_M modulated by deformation stress σ. As a representative plot, the magnetization isotherms of Mn_5Ge_3 at $\sigma = 0$ GPa and $\sigma = 0.75$ GPa are shown in Figs. 3(a) and 3(b), and the results under other stresses are shown in Fig. S5. From the magnetization isotherms, we calculate the corresponding values of $-\Delta S_M$ as a function of temperature and field changes. The results are presented in Figs. 3(c) and 3(d), and the results under other stresses are shown in Fig. S6. The applied external magnetic field H parallels the [0001] direction for all the measurements, as indicated in Fig. 3(a). The value of maximum magnetic entropy change ($-\Delta S_M^{max} = 3.5$ J/kg·K) at $\sigma = 0$ GPa for $\Delta H = 1.6$ T is close to that reported in Ref. [12]. It is worth noting that the value of $-\Delta S_M^{max}$ at $\sigma = 0.75$ GPa can reach 5.6 J/kg·K for $\Delta H = 1.6$ T. Table 1 enumerates the comparative analysis of this compound relative to other similar compounds.

Figure 3(e) plots the σ dependence of $-\Delta S_M^{max}$ for Mn_5Ge_3. It can be seen that with the increase of σ, the magnitude of $-\Delta S_M^{max}$ does not monotonically increase but shows a peak shape and reaches a peak value of 5.6 J/kg·K at $\sigma = 0.75$ GPa. This result has a significant 60% improvement over that of $\sigma = 0$ GPa at peak temperature of $T_{peak} = 300$ K. This value is even 115% higher than the magnetic entropy change of the polycrystalline sample [Fig. 3(f)] and is comparable to Gd ($-\Delta S_M^{max} = 6.0$ J/kg·K, $\Delta H = 2.0$ T), which has

been used as a benchmark material in magnetic refrigerator prototypes.[41] It is worth noting that the value of $-\Delta S_M^{max}$ does not show a monotonical increase trend with the increase of strain energy density [Fig. 2(c)]. This may be due to a deterioration in magnetization caused by poly-crystallization and the appearance of other phases after deformation of $\sigma > 0.75$ GPa, as discussed in the section of Fig. 2.

To verify the accuracy of the above experimental results, we perform the field dependence of the magnetic entropy change. For SOMT materials, the field dependence of the $-\Delta S_M^{max}$ follows the power law:[42,43] $-\Delta S_M^{max} \propto H^n$, where n is the power exponent associated with temperature and applied external magnetic field. The field dependence of magnetic entropy change has the following empirical features:[42] for temperatures well below Curie temperature (T_C), $n = 1$; well above T_C, $n = 2$; and at the peak temperature corresponding to $-\Delta S_M^{max}$, $n \approx 0.75$. In our case, the value of n varies between 1 and 2 with temperature for all the samples before and after deformation (Fig. S8). Figure 4(a) shows the temperature dependence of n for the as-prepared sample ($\sigma = 0$ GPa) and deformed sample ($\sigma = 0.75$ GPa). Insets show the fitting results by the power law at the peak temperature corresponding to $-\Delta S_M^{max}$ of $T_{pk} = 300$ K. For the as-prepared sample, $n = 0.75$ at $T_{pk} = 300$ K. This value agrees with the above empirical features. For the deformed sample, $n = 0.83$ at $T_{pk} = 300$ K, slightly higher than 0.75. Considering that the value of n at $T = 297$ K is only 0.70, this result may be caused by rapid changes in ΔS_M over a very narrow temperature range.

Figure 4(b) shows the temperature dependence of magnetization with different stress ($\sigma = 0$ GPa and 0.75 GPa) of the Mn_5Ge_3 single crystals at $H = 500$ Oe (1 Oe = 79.5775 A·m^{-1}). The field cooling (FC) and zero-field cooling (ZFC) curves almost coincide, indicating no thermal hysteresis in our samples. The corresponding derivatives of the FC curves demonstrate that the Curie temperature of the as-prepared and deformed samples are 298 K and 299 K [the inset of Fig. 4(b)].

To further explain the mechanism of strain energy enhancing magnetization in Mn_5Ge_3, we perform Monte Carlo simulations using the Ising-like Hamiltonian[28,44]

$$H = -\sum_{i \neq j} J_{ij} \boldsymbol{S}_i \cdot \boldsymbol{S}_j - \boldsymbol{h} \cdot \sum_i g_i \boldsymbol{S}_i - E_u, \tag{2}$$

where J_{ij} is the exchange constant between the spins $\boldsymbol{S}_i$ and $\boldsymbol{S}_j$, $\boldsymbol{hh}$ is the external magnetic field, g_i is the Lande factor, and E_u is the strain energy. Figure 4(c) shows the simulated $-\Delta M/\Delta T$ of Mn_5Ge_3 at $\Delta T = 5\ J_{dd}$. With increasing E_u, the value of $-\Delta M/\Delta T$ has an apparent tendency to increase. This result is consistent with the trend of our experimental results and strongly indicates that the ΔS_M of Mn_5Ge_3 can be intentionally tuned by the introduction of strain energy.

4. Conclusion

In summary, we realize a significant 60% improvement in the magnetic entropy change at room temperature in Mn_5Ge_3 single crystals by introducing microscopic strain and lattice deformation with high-pressure constrained deformation. Both theoretical simulations and experimental results demonstrate that the prominent increase in magnetic entropy change originates from the tunable strain energy introduced by deformation. This additional strain energy will reconstruct the energy landscape of this ferromagnetic system and generate an enhancement in magnetization, resulting in a giant intensity of magnetocaloric responses. Our results provide an approach to increase magnetic entropy change and may give fresh ideas for exploring advanced magnetocaloric materials.

Acknowledgements

The authors would like to thank Dr. Jie Ren for his assistance in the Monte Carlo simulations. Project supported by the National Key Research and Decelopment Program of China (Grant No. 2021YFB3500302), the National Natural Science Foundation of China (Grant Nos. U22A20116 and 52371200), and the Innovation Capability Improvement Project of Hebei Province, China (Grant No. 22567605H).

References

[1] Shen B G, Sun J R, Hu F X, Zhang H W and Cheng Z H 2009 *Adv. Mater.* **21** 4545
[2] Gutfleisch O, Willard M A, Brück E, Chen C H, Sankar S G and Liu J P 2011 *Adv. Mater.* **23** 821
[3] Xiang J S, Zhang C D, Gao Y, Schmidt W, Schmalzl K, Wang C W, Li B, Xi N, Liu X Y, Jin H, Li G, Shen J, Chen Z Y, Qi Y, Wan Y, Jin W T, Li W, Sun P J and Su G 2024 *Nature* **625** 270
[4] Levinsky J J B, Beckmann B, Gottschall T, Koch D, Ahmadi M, Gutfleisch O and Blake G R 2024 *Nat. Commun.* **15** 8559
[5] Brown G V 1976 *J. Appl. Phys.* **47** 3673
[6] Franco V, Blázquez J S, Ingale B and Conde A 2012 *Annu. Rev. Mater. Res.* **42** 305
[7] Gottschall T, Skokov K P, Fries M, Taubel A, Radulov I, Scheibel F, Benke D, Riegg S and Gutfleisch O 2019 *Adv. Eng. Mater.* **9** 1901322
[8] Zarkevich N A and Zverev V I 2020 *Crystals* **10** 815
[9] Law J Y, Franco V, Moreno-Ramírez L M, Conde A, Karpenkov D Y, Radulov I, Skokov K P and Gutfleisch O 2018 *Nat. Commun.* **9** 2680
[10] Law J Y, Moreno-Ramírez L M, Díaz-García Á and Franco V 2023 *J. Appl. Phys.* **133** 040903
[11] Singh S, Caron L, D'Souza S W, Fichtner T, Porcari G, Fabbrici S, Shekhar C, Chadov S, Solzi M and Felser C 2016 *Adv. Mater.* **28** 3321
[12] Wang S B, Fan C Z and Liu D M 2021 *ACS Appl. Mater. Inter.* **13** 33237
[13] Li L W, Nishimura K, Hutchison W D, Qian Z H, Huo D X and NamiKi T 2012 *Appl. Phys. Lett.* **100** 152403
[14] Xi S B, Lu W J and Sun Y P 2012 *J. Appl. Phys.* **111** 063922
[15] Belyea D D, Lucas M S, Michel E, Horwath J and Miller C W 2015 *Sci. Rep.* **5** 15755
[16] Hao J Z, Hu F X, Zhou H B, Liang W H, Yu Z B, Shen F R, Gao Y H, Qiao K M, Li J, Zhang C, Wang B J, Wang J, He J, Sun J R and Shen B G 2020 *Scripta Mater.* **186** 84
[17] Liu J 2014 *Chin. Phys. B* **23** 047503
[18] Yin H, Law J Y, Huang Y J, Shen H X, Jiang S D, Guo S, Franco V and Sun J F 2022 *Sci. China Mater.* **65** 1134
[19] Zhang X Y, Hua Y X and Li X H 2025 *Sci. China Phys. Mech. Astron.* **68** 247511

[20] Hua Y X, Li X H, Li J X, Luo X, Li Y Q, Qin W Y, Zhang L Q, Xiao J W, Xia W X, Song P, Yue M, Zhang H T and Zhang X Y 2024 *Science* **385** 634

[21] Li X H, Lou L, Song W P, Huang G W, Hou F C, Zhang Q, Zhang H T, Xiao J W, Wen B and Zhang X Y 2017 *Adv. Mater.* **29** 1606430

[22] Lou L, Li Y Q, Li X H, Li H L, Li W, Hua Y X, Xia W X, Zhao Z H, Zhang H T, Yue M and Zhang X Y 2021 *Adv. Mater.* **33** 2102800

[23] Li X H, Lou L, Song W P, Zhang Q, Huang G W, Hua Y X, Zhang H T, Xiao J W, Wen B and Zhang X Y 2017 *Nano Lett.* **17** 2985

[24] Li W, Li L L, Nan Y, Li X H, Zhang X Y, Gunderov D V, Stolyarov V V and Popov A G 2007 *Appl. Phys. Lett.* **91** 062509

[25] Liu Y G, Xu L, Wang Q F, Li W and Zhang X Y 2009 *Appl. Phys. Lett.* **94** 172502

[26] Li H L, Lou L, Hou F C, Guo D F, Li W, Li X H, Gunderov D V, Sato K and Zhang X Y 2013 *Appl. Phys. Lett.* **103** 142406

[27] Zhang X Y 2020 *Heterostructures: new opportunities for functional materials Mater. Res. Lett.* **8** 49

[28] Song P, Yao S, Zhang B X, Jiang B, Deng S S, Guo D F, Ma L and Hou D L 2022 *Appl. Phys. Lett.* **120** 192401

[29] Huang G W, Li X H, Lou L, Hua Y X, Zhu G J, Li M, Zhang H T, Xiao J W, Wen B, Yue M and Zhang X Y 2018 *Small* **14** 1800619

[30] Picozzi S, Continenza A and Freeman A J 2004 *Phys. Rev. B* **70** 235205

[31] Songlin, Dagula, Tegus O, Brück E, De Boer F R and Buschow K H J 2002 *J. Alloys Compd.* **337** 269

[32] Maraytta N, Voigt J, Salazar Mejía C, Friese K, Skourski Y, Perßon J, Salman S M and Brückel Th 2020 *J. Appl. Phys.* **128** 103903

[33] Lalita, Rathi A, Pardeep, Verma A K, Gahtori B, Gautam A, Pant R P, Babu P D and Basheed G A 2021 *J. Alloys Compd.* **876** 159908

[34] Zhao M Y, Guo W, Wu X, Ma L, Song P, Li G K, Zhen C M, Zhao D W and Hou D L 2023 *Mater. Horiz.* **10** 4597

[35] Selinger J V 2016 *Introduction to the theory of soft matter: From ideal gases to liquid crystals* (Cambridge: Springer International Publishing) pp. 7–23

[36] Biju V, Sugathan N, Vrinda V and Salini S L 2008 *J. Marer. Sci.* **43** 1175

[37] Yang T H, He W, Chen F K and He C Y 2022 *J Magn Magn Mater.* **559** 169539

[38] Gschneidner Jr K A and Pecharsky V K 2000 *Annu. Rev. Mater. Sci.* **30** 387

[39] Zhao F Q, Dagula W, Tegus O and Buschow K H J 2006 *J. Alloys Compd.* **416** 43

[40] Zheng T F, Shi Y G, Fan J Y, Shi D N, Tang S L, Lv L Y and Zhong W 2013 *J. Appl. Phys.* **113** 17

[41] Gschneidner K A and Pecharsky V K 2000 *Annu. Rev. Mater. Sci.* **30** 387

[42] Franco V, Blázquez J S and Conde A 2006 *F Appl. Phys. Lett.* **89** 222512

[43] Lalita, Babu P D, Pardeep and Basheed G A 2023 *Alloy J. Appl. Phys.* **134** 173903

[44] Ghediri A, Chiba Y and Tlemçani A 2022 *Artificial Intelligence and Heuristics for Smart Energy Efficiency in Smart Cities* (Cambridge: Springer International Publishing) pp. 847–856